Magneto-optical properties of Cr³⁺ in β-Ga₂O₃

Jan E. Stehr¹*, Mattias Jansson¹, Quanzheng Tao¹, Detlev M. Hofmann², Jihyun Kim³, Stephen J. Pearton⁴, Weimin M. Chen¹, and Irina A. Buyanova^{1‡}

¹ Department of Physics, Chemistry and Biology, Linköping University, 58183 Linköping, Sweden

² Physikalisches Institut, Justus-Liebig-University Giessen, Heinrich-Buff-Ring 16, 35392 Giessen, Germany

³Department of Chemical and Biological Engineering, Korea University, Seoul 136-713, Korea

⁴Department of Materials Science and Engineering, University of Florida, Gainesville, Florida 32611, USA

Corresponding authors:

*Jan E. Stehr (jan.eric.stehr@liu.se)

[‡] Irina A. Buyanova (irina.bouianova@liu.se)

ABSTRACT

β-Ga₂O₃ is a wide bandgap semiconductor that is attractive for various applications, including in power electronics and for transparent conductive electrodes. Its properties can be strongly affected by transition metal impurities commonly present during the growth, such as Cr. In this letter we determine the electronic structure of Cr³⁺ by performing a correlative study of magneto-photoluminescence (magneto-PL) and electron paramagnetic resonance (EPR). We unambiguously prove that the so-called R₁ and R₂ PL lines at around 1.79 eV originate from an

internal transition between the first excited state (2E) and the 4A_2 ground state of Cr^{3+} . The center is concluded to have monoclinic local symmetry and exhibits a large zero-field splitting (~ 146 µeV) of the ground state, which can be directly measured from fine structure of the R1 transition. Furthermore, g-values of the first excited state are accurately determined as $g_a = 1.7$, $g_b = 1.5$ and $g_{c^*} = 2.1$. Our results advance our understanding of the electronic structure of Cr in β -Ga₂O₃ and provide a spectroscopic signature of this common residual impurity.

Keywords

Gallium Oxide, electron paramagnetic resonance, magneto-PL, impurities, Cr³⁺

β-Ga₂O₃ is a newly emerging wide bandgap semiconductor with a bandgap energy of 4.7 eV at room temperature that has a higher figure of merit for power electronics than the commonly used GaN and SiC materials due to a higher breakdown field^{1,2}. Furthermore, it has attracted considerable attention for applications as transparent conductive electrodes, solar-blind UV photodetectors^{3,4}, gas sensors^{5,6}, and for photoelectrochemical water splitting^{7,8}. Large β-Ga₂O₃ bulk crystals can be manufactured with a high quality and a reasonable price by melt growth techniques, which is a prerequisite for the fabrication of industrial scale high-performance power devices and other applications. For all device applications, it is a necessity to have a reliable control over electrical and optical properties of the material. Though this can be achieved by controlled doping during the growth, doping efficiency is often strongly affected by unintentional doping caused by contaminants in the starting material. An important group of such unintentional impurities are transition-metal ions, which are often present during the growth and mostly form deep-level states in β-Ga₂O₃ limiting its electrical conductivity^{9–13}. Moreover, these transitionmetal impurities can be used as intentional dopants required to compensate intrinsic n-type doping and achieve a semi-insulating material. Under proper doping conditions, they may also induce ferromagnetism in β-Ga₂O₃, ¹⁴ promising for spintronic applications. Therefore, it is of crucial importance to identify the electronic structure of these impurities that can lead to a better understanding and prediction of their effects on electrical and optical properties of the material. It is also useful to obtain a reliable and straight-forward spectroscopic signature of a specific transition-metal impurity that can be used for its easy identification using standard characterization techniques, e.g. photoluminescence (PL) spectroscopy.

One of the common transition-metal impurities in β -Ga₂O₃ is Cr^{15,16}. Previous electron paramagnetic resonance (EPR) studies¹⁷⁻¹⁹ have provided spin-Hamiltonian parameters of the

ground state of Cr in the 3+ charge state (Cr^{3+}), though the sign of the zero-field-splitting (ZFS) parameters is still uncertain and differs between the reports. Also controversial is an optical signature of Cr^{3+} , since the direct experimental proof of Cr involvement in any optical transitions is currently lacking. It was first suggested ¹⁹⁻²¹ that internal transitions of Cr^{3+} give rise to two sharp emission (or absorption) lines at around 1.78 eV and 1.80 eV at room temperature (RT), which were labeled as R1 and R2 lines ^{16,19-24}. This conclusion was based on a similarity of the transition energies with the internal transitions of Cr^{3+} in Al_2O_3 , ^{25,26} as well as on the analysis of absorption spectra of Cr-doped β - Ga_2O_3 using the Tanabe–Sugano diagrams ²⁷. The same emission, however, was also attributed ²⁸ to the ⁴T₁ \rightarrow ⁶A₁ intracenter transition of Fe^{3+} , since the dramatic enhancement of the emission intensity was observed upon Fe doping.

To determine the exact electronic states and thereby definitely identify the chemical origin of the transition-metal impurity responsible for the R-line emissions in β -Ga₂O₃, it is essential to resolve and determine the spin degeneracy of both excited and ground state. In this work we carry out a detailed study by combining the EPR spectroscopy, which can determine the spin states of the ground state, with magneto-PL that is sensitive to both excited and ground state. Based on the observed splitting of the R1 emission in an applied magnetic field we unambiguously show that the R-lines originate from the internal ${}^2E \rightarrow {}^4A_2$ transitions of the Cr³⁺ center that has a monoclinic local symmetry. We obtain accurate spin-Hamiltonian parameters of its ground state (4A_2) as well as previously unknown g-values of the first excited state (2E).

We used commercially available undoped β -Ga₂O₃ bulk crystals from Tamura and undoped β -Ga₂O₃ bulk crystals grown by the Czochralski method²⁹. The crystallographic axes a, b and c* of the samples were determined by x-ray diffraction analysis. For magneto-PL experiments the samples were placed inside a cryostat equipped with a superconducting magnet, operating between

0 and 5 T. The sample temperature could be varied between 7 K and RT. The measurements were performed in the backscattering geometry, so that the magnetic field was parallel to the light excitation and collection axis. A solid-state 532-nm laser was used as an excitation source. The laser light was focused on the sample surface using a 50X (NA=0.5) objective lens, which was also used to collect PL. The PL was dispersed through a single-grating monochromator and detected using a Si charge coupled device. EPR experiments were performed in dark using a Bruker E500 EPR spectrometer equipped with a X-band resonator and a He-gas flow cryostat for measurements with adjustable temperatures ranging between 5 K and 300 K.

To evaluate unintentional doping of the investigated samples we first performed EPR measurements. Figure 1 (a) and (d) depict EPR spectra measured at 6 K with an applied magnetic field B parallel to the crystallographic b-axis, when the sample was mounted with the rotation axis perpendicular to the (ab) and (bc^*) plane, respectively. EPR spectra obtained under $B \parallel a$ and $B \parallel c^*$ are shown in Fig. 1 (c) and (f), respectively. c^* denotes a complementary axis that is orthogonal to the a and b axes. In addition to the previously observed signals from Co^{2^+} with a $3d^7$ ground state and an effective electron spin $S_{\rm eff} = 1/2^{-13}$ and a shallow donor (SD) 17,18,30 , all spectra contain a highly anisotropic signal consisting of two lines located at 130 and 1315 mT when $B \parallel b$. Spin-Hamiltonian parameters of this signal can be obtained from angular dependent EPR measurements. Results of these measurements are summarized in Fig. 1 (b) and (e), where the measured peak positions (the open symbols) are shown as a function of the angle θ between B and the a-axis for rotations in the (ab) plane and the c^* -axis for rotations in the (bc^*) plane as indicated in the insets. We analyze these data using the following spin-Hamiltonian:

$$\mathcal{H} = \mu_B B g S + B_2^0 O_2^0 + B_2^2 O_2^2 + B_2^1 O_2^1$$
 (1).

Here, the first term is the electron Zeeman term with \mathbf{g} being the electron g-tensor and μ_B the Bohr magneton. To describe ZFS in the monoclinic crystal structure in an easier manner, we use the extended Stevens operators in the form of O_k^q with the ZFS parameters B_k^q 31. The ZFS is then described by the sum of an orthorhombic component ($B_2^0O_2^0 + B_2^2O_2^2$) and a monoclinic component ($B_2^1O_2^1$). By fitting the spin Hamiltonian to the experimental data using the Easyspin software package³², we extract the full set of spin-Hamiltonian parameters given in Table 1. The simulated angular dependences are shown by the solid lines in Fig.1 (b) and (e) and are in excellent agreement with the experimental data. The extracted parameters are typical^{31,33,34} for a Cr³⁺ ion with the 3d³ electron configuration (S=3/2) that substitutes for a Ga³⁺ ion (likely at the orthorhombic site) and has a monoclinic local symmetry. We note that in the literature the ZFS sign is uncertain and differs among reports. We accurately determine the sign from magneto-PL measurements, as will be described below. The EPR experiments clearly prove trace contamination by Cr of the investigated samples. Another transition-metal impurity, which could also be detected by EPR in some of our samples, is Fe³⁺ in the 3d⁵ configuration with S=5/2 (not present in the sample shown in Fig.1).

We now analyze optical properties of the investigated samples. Under the 532-nm excitation, all of them show bright R-line emissions commonly observed in β-Ga₂O₃ ^{20,23,28,34} – see Fig. 2(a). Both the R₁ and the R₂ lines are observed at 300 K, whereas only the R₁ transition can be detected at 5K. This suggests that the R2 transition stems from a higher-lying excited state of a transition metal, consistent with previous studies^{19,20,22}. At 5K, the R1 line has a very narrow linewidth with a full width at half maximum (FWHM) of around 88 μeV. This linewidth, however, is determined by an inhomogeneous broadening since the R1 lifetime at this temperature is known to be around several ms^{19,20,22}. The narrow linewidth has enabled us to uncover that the R1 line in fact contains two components split by 146 μeV at zero magnetic field, as shown in Fig.2(b)-2(d). Since no

thermalization between these components is observed in PL, the detected ZFS must occur in the ground state. We note that the observation of this splitting, which was not resolved previously, allows us to accurately measure the ZFS energy of the ground state without relying on any fitting procedure. Application of an external magnetic field **B** causes further splitting of the R1 doublet into eight components labeled as 1 - 8, in the order of increasing energy. This can be seen from Figure 2(b)-(d), which depict evolution of magneto-PL spectra with increasing \mathbf{B} that were measured at 5K with $\boldsymbol{B} \parallel a$ (b), $\boldsymbol{B} \parallel b$ (d) and $\boldsymbol{B} \parallel c^*$ (c). In order to determine whether the magneticfield induced splitting occurs in the ground or excited state, temperature-dependent PL measurements were performed at B=5T. The results of such measurements for $\boldsymbol{B} \parallel a$ are shown in the inset of Fig. 2(e). We also plot the difference between the PL spectra obtained at 5K and 20K, for more clarity. It is found that four transitions (labeled as 2, 4, 6, and 8) gain intensity at elevated temperatures, which clearly proves that they stem from the same, higher-lying spin sublevel of the excited state, which becomes thermally populated. The observation of two groups of four lines also shows that: (i) the excited state of the transition metal ion involved in the R1 transition is twofold spin degenerate with the electron spin S=1/2; (ii) the ground state is fourfold degenerate with S=3/2. We can then extract the energy difference ΔE of the two spin sublevels of the excited state, i.e. the Zeeman splitting, which is plotted in Figure 2(e) as a function of **B**. Linear dependences of $\Delta E(B)$ are observed for all three orientations of the applied magnetic field relative to the crystallographic axes. By fitting them with the Zeeman splitting term $\Delta E = \mu_B BgS$ with S= 1/2, the g-values of the excited state can be deduced as $g_a=1.7,\,g_b=1.5$ and $g_{c^*}=2.1.$

Knowing the g-values of the excited state, fan diagrams of the ground state can be obtained. The corresponding results for $B \parallel a$, $B \parallel b$ and $B \parallel c^*$ are shown by the open symbols in Fig. 3(a), (b) and (c), respectively. The experimental data can be fitted by Eq. 1 using the spin-Hamiltonian

parameters that were obtained from the EPR experiments (see Table 1). The simulation results are shown in Fig.3 by the solid lines and are in excellent agreement with the experiment. This unambiguously proves that Cr^{3+} is the origin of the R-lines commonly observed in absorption and emission spectra of β -Ga₂O₃. Furthermore, careful inspection of the data at high magnetic fields B>3T shows that the equidistant splitting between four spin sublevels of the ground state is observed only when $B \parallel a$ (Fig.3(a)). On the other hand, it is the largest for two lowest sublevels when $B \parallel b$ - see Fig.3(b) and for the two upmost sublevels when $B \parallel c^*$ - see Fig. 3(c). Such behavior can only be modeled assuming that the ZFS parameters have a positive sign.

In Fig.4 we summarize the obtained results by using the following energy level diagram of the intracenter transitions responsible for the R lines. In a cubic lattice, substitutional Cr^{3+} ions in a $3d^3$ electron configuration have the fourfold degenerate ground state 4A_2 and the fourfold degenerate first excited state 2E . In β -Ga $_2$ O $_3$ with monoclinic symmetry, both ground and excited states exhibit zero field splittings due to combined effects of the monoclinic crystal field, spinorbit and spin–spin interactions. The R-lines are related to the $^2E \rightarrow ^4A_2$ transitions, as was suggested previously but is only proven in the present study. The 18.6 meV splitting between the R1 and R2 transitions defines the splitting between the two Kramers' doublets forming the 2E state. The 4A_2 state also splits into two doublets and the related ZFS energy (δ) can be directly measured from the fine structure of the R1 emission resolved at low temperatures – see Fig.2. The δ value of 146 μ eV measured by PL is in excellent agreement with 149 μ eV deduced from the EPR analysis. The suggested spin degeneracy of the involved states is directly confirmed by the magneto-PL data. Under an external magnetic field, the lower-lying doublet of the 2E excited state splits into two spin sublevels, whereas the 4A_2 ground state splits into four sublevels – see Fig.4.

This gives rise to eight components of the R1 emission that are labelled in Fig. 4 according to the labeling used in Fig.3.

In conclusion, by using magneto-PL spectroscopy combined with EPR measurements we have identified the electronic structure and spin configuration of the Cr^{3+} ion in β -Ga₂O₃. We provided unambiguously evidence that the intracenter transitions between the 2E excited state and the 4A_2 ground state of Cr^{3+} are responsible for the R_1 and R_2 PL lines at around 1.79 eV commonly seen in β -Ga₂O₃, based on the identical spin-Hamiltonian parameters of the ground state involved in the R1 emission measured by both techniques. The Cr^{3+} center is concluded to have monoclinic local symmetry and exhibits a large ZFS of $\sim 146~\mu eV$ in the ground state, which can be directly measured from the splitting of the R1 transition at low temperatures. Furthermore, the spin-Hamiltonian parameters of the ground state and the lowest-lying excited state are accurately determined. Our results have, therefore, contributed to a better understanding of the electronic structure of Cr in β -Ga₂O₃. They also provide a spectroscopic signature of this impurity and show that the presence of Cr can be easily and reliably traced from simple PL measurements performed at room temperature under optical excitation with commonly available light sources emitting, e.g. within the green spectral range.

Acknowledgements

We would like to thank Leibniz-Institut für Kristallzüchtung (Berlin) for providing the β-Ga₂O₃ bulk crystal sample. Financial support by Linköping University through the Professor Contracts and the Swedish Government Strategic Research Area in Materials Science on Functional Materials at Linköping University (Faculty Grant SFO-Mat-LiU No 2009 00971) is greatly

appreciated. The work at UF was supported by the Interaction of Ionizing Radiation with Matter University Research Alliance (IIRM-URA), sponsored by the Department of the Defense, Defense Threat Reduction Agency under award HDTRA1-20-2-0002 and also by NSF DMR 1856662 (James Edgar).

Notes

J.E.S. and M.J. contributed equally to this work.

References:

- ¹ S.J. Pearton, J. Yang, P.H. Cary, F. Ren, J. Kim, M.J. Tadjer, and M.A. Mastro, Appl. Phys. Rev. **5**, 011301 (2018).
- ² M. Baldini, Z. Galazka, and G. Wagner, Mater. Sci. Semicond. Process. **78**, 132 (2018).
- ³ A.S. Pratiyush, S. Krishnamoorthy, R. Muralidharan, S. Rajan, and D.N. Nath, in *Gall. Oxide* (Elsevier, 2019), pp. 369–399.
- ⁴ X. Hou, Y. Zou, M. Ding, Y. Qin, Z. Zhang, X. Ma, P. Tan, S. Yu, X. Zhou, X. Zhao, G. Xu, H. Sun, and S. Long, J. Phys. D. Appl. Phys. **54**, 043001 (2021).
- ⁵ S. Kumar and R. Singh, Phys. Status Solidi Rapid Res. Lett. 7, 781 (2013).
- ⁶ T.F. Weng, M.S. Ho, C. Sivakumar, B. Balraj, and P.F. Chung, Appl. Surf. Sci. **533**, 147476 (2020).
- ⁷ R. Ito, M. Akatsuka, A. Ozawa, Y. Kato, Y. Kawaguchi, M. Yamamoto, T. Tanabe, and T. Yoshida, ACS Omega **4**, 5451 (2019).
- ⁸ X. Qiu, J. Zhang, H. Dong, and X. Zhou, Theor. Chem. Acc. **136**, 79 (2017).
- ⁹ M.L. Meil'Man and I.A. Gavrilov, Sov. Phys. Sol. State 11, 628 (1969).
- ¹⁰ V. Folen, Phys. Rev. **139**, A1961 (1965).
- ¹¹ I.G. Kim, T.H. Yeom, S.H. Lee, Y.M. Yu, H.W. Shin, and S.H. Choh, J. Appl. Phys. **89**, 4470 (2001).
- ¹² L. Binet, D. Gourier, and C. Minot, J. Solid State Chem. **113**, 420 (1994).
- ¹³ J.E. Stehr, D.M. Hofmann, J. Schörmann, M. Becker, W.M. Chen, and I.A. Buyanova, Appl. Phys. Lett. **115**, 242101 (2019).
- ¹⁴ K. Ichihashi, H. Shinya, and H. Raebiger, Appl. Phys. Express **13**, 021002 (2020).
- ¹⁵ C.A. Lenyk, T.D. Gustafson, L.E. Halliburton, and N.C. Giles, J. Appl. Phys. **126**, 245701 (2019).
- ¹⁶ G. Naresh-Kumar, H. MacIntyre, S. Subashchandran, P.R. Edwards, R.W. Martin, K. Daivasigamani, K. Sasaki, and A. Kuramata, Phys. Status Solidi 258, 2000465 (2021).
- 17 M. Yamaga, iacute, E. Ilora, oacute, G. n, K. Shimamura, N. Ichinose, and M. Honda, Phys. Rev. B $\bf 68$, 155207 (2003).
- ¹⁸ N.T. Son, K. Goto, K. Nomura, Q.T. Thieu, R. Togashi, H. Murakami, Y. Kumagai, A. Kuramata, M. Higashiwaki, A. Koukitu, S. Yamakoshi, B. Monemar, and E. Janzén, J. Appl. Phys. **120**, 235703 (2016).
- ¹⁹ H. Tippins, Phys. Rev. **137**, A865 (1965).
- ²⁰ R. Sun, Y.K. Ooi, P.T. Dickens, K.G. Lynn, and M.A. Scarpulla, Appl. Phys. Lett. **117**, 052101 (2020).
- ²¹ T. Yoshinori and A. Sadao, J. Appl. Phys. **112**, 063522 (2012).
- ²² D. Vivien, B. Viana, A. Revcolevschi, J.D. Barrie, B. Dunn, P. Nelson, and O.M. Stafsudd, J.

- Lumin. 39, 29 (1987).
- ²³ E. Nogales, J.A. García, B. Méndez, and J. Piqueras, J. Appl. Phys. **101**, 033517 (2007).
- ²⁴ X. Lu, S. Venugopalan, H. Kim, M. Grimsditch, S. Rodriguez, and A.K. Ramdas, Phys. Rev. B Condens. Matter Mater. Phys. **79**, 235204 (2009).
- ²⁵ S. Sugano and I. Tsujikawa, J. Phys. Soc. Japan **13**, 899 (1958).
- ²⁶ H. Hori, H. Mollymoto, and M. Date, J. Phys. Soc. Japan **46**, 908 (1979).
- ²⁷ Y. Tanabe and S. Sugano, J. Phys. Soc. Japan **9**, 753 (1954).
- ²⁸ A.Y. Polyakov, N.B. Smirnov, I. V. Schemerov, A. V. Chernykh, E.B. Yakimov, A.I. Kochkova, A.N. Tereshchenko, and S.J. Pearton, ECS J. Solid State Sci. Technol. **8**, Q3091 (2019).
- ²⁹ Z. Galazka, R. Uecker, K. Irmscher, M. Albrecht, D. Klimm, M. Pietsch, M. Brützam, R. Bertram, S. Ganschow, and R. Fornari, Cryst. Res. Technol. **45**, 1229 (2010).
- ³⁰ J. Vincent, O. Guillot-Noël, L. Binet, P. Aschehoug, Y. Le Du, F. Beaudoux, and P. Goldner, J. Appl. Phys. **104**, 033519 (2008).
- ³¹ A. Abragam and B. Bleaney, *Electron Paramagnetic Resonance of Transition Ions* (Clarendon, P., 1970).
- ³² S. Stoll and A. Schweiger, J. Magn. Reson. **178**, 42 (2006).
- ³³ T.H. Yeom, I.G. Kim, S.H. Lee, S.H. Choh, and Y.M. Yu, J. Appl. Phys. **93**, 3315 (2003).
- ³⁴ W. Gunsser and K. Rohwer, Phys. Status Solidi **116**, 275 (1983).
- ³⁵ E. Nogales, B. Méndez, and J. Piqueras, Appl. Phys. Lett. **86**, 113112 (2005).

Figures:

Figure 1:

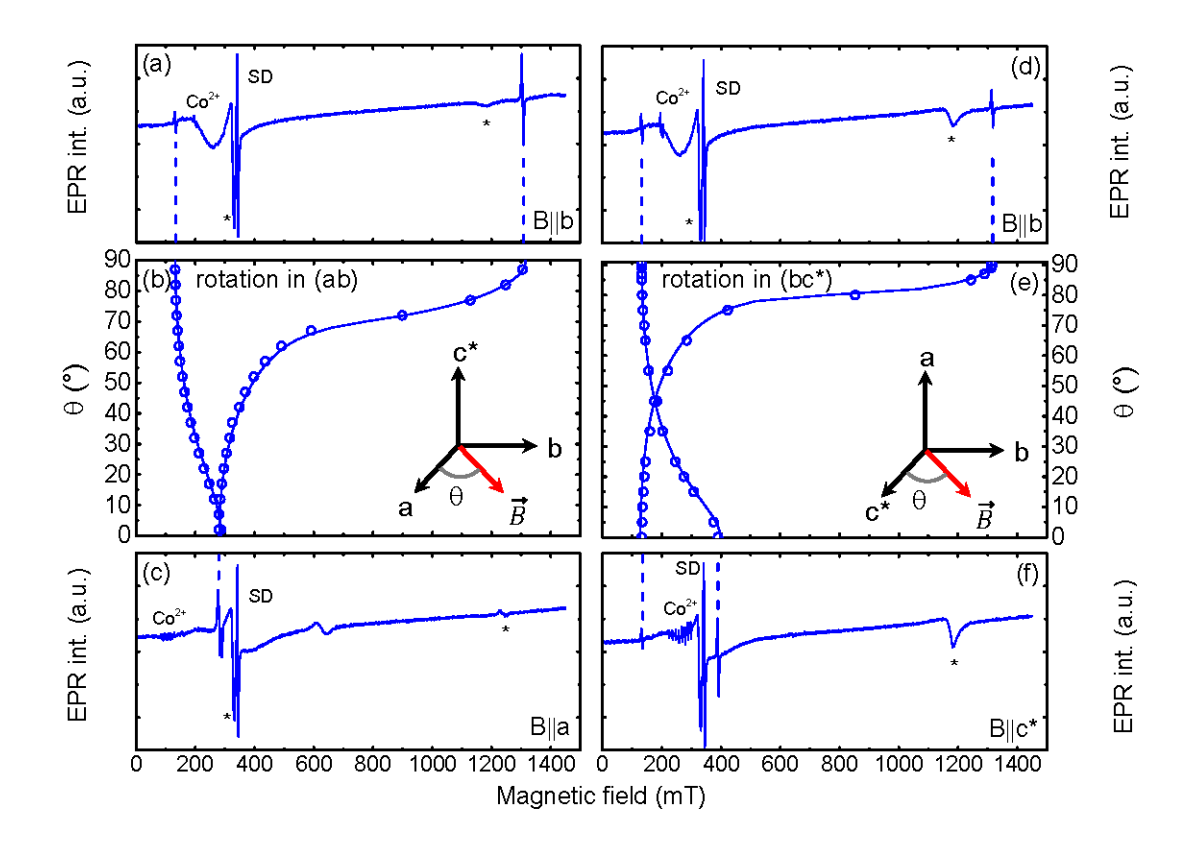


Figure 2:

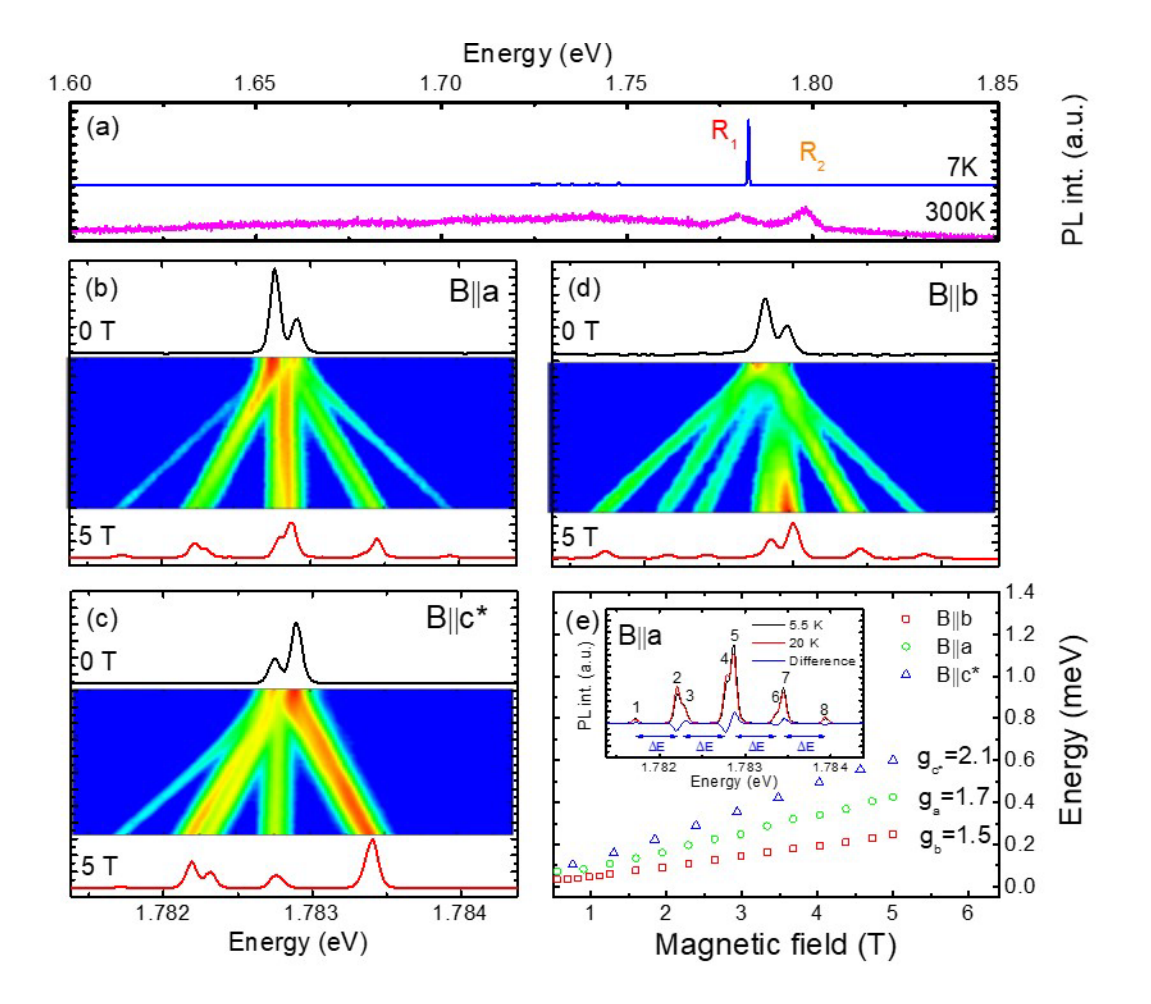


Figure 3:

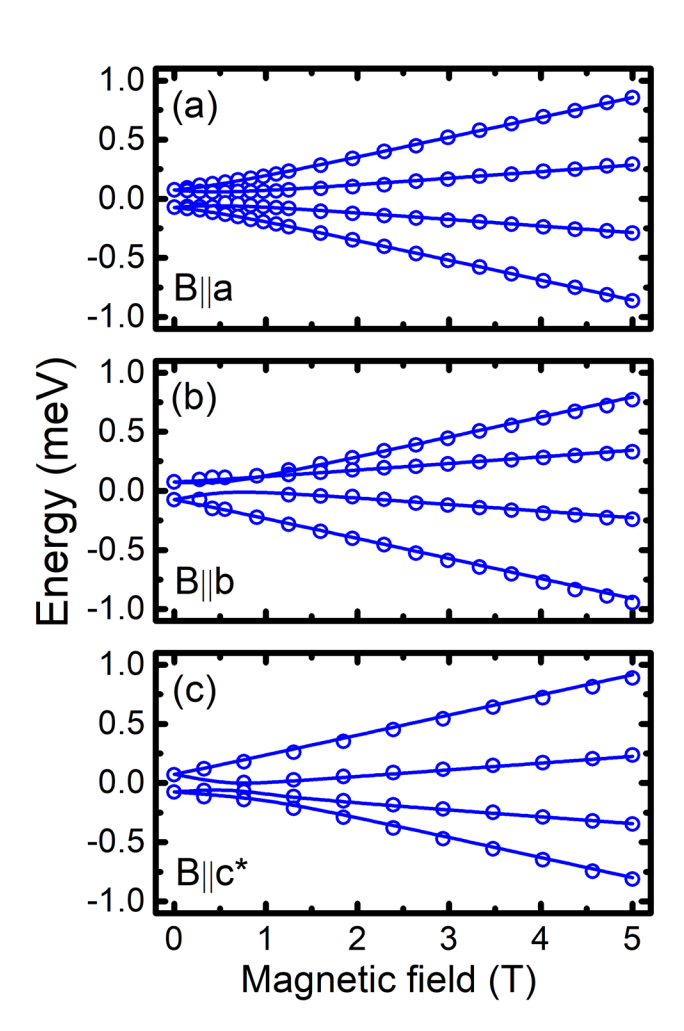


Fig. 4:

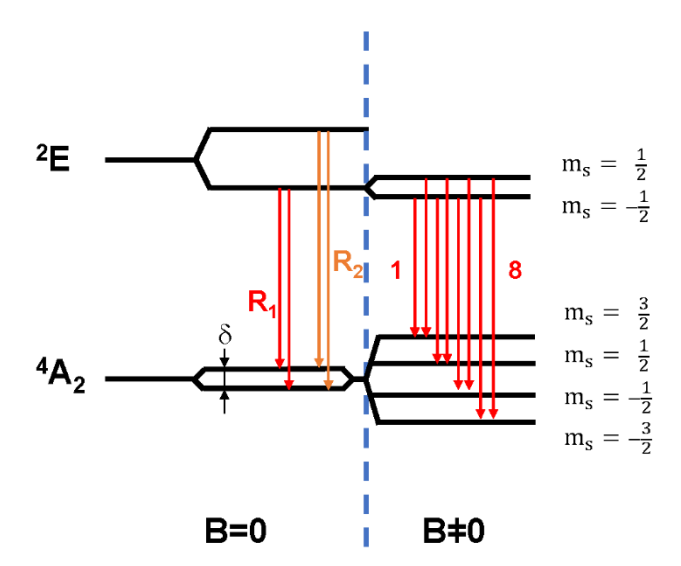


Table 1: Summary of the spin-Hamiltonian parameters of Cr^{3+} in β -Ga₂O₃ responsible for the R₁ emission.

State	S	g-tensor	B_k^q (MHz)
Ground state	3/2	$g_a = 1.96 \pm 0.005$	$B_2^0 = 4750 \pm 30$
		$g_b = 1.96 {\pm} 0.005$	$B_2^2 = 4700 \pm 30$
		$g_{c^*} = 1.97{\pm}0.005$	$B_2^1 = 8650 \pm 30$
Lowest excited state	1/2	$g_a=1.7{\pm}0.05$	
		$g_b=1.5{\pm}0.05$	
		$g_{c^*} = 2.1 \pm 0.05$	

Figure captions:

Figure 1: EPR spectra from bulk β -Ga₂O₃ with an applied magnetic field **B** parallel to the crystallographic *b*-axis (a,d), *a*-axis (c) and *c**-axis (f). (b) and (e) depict angular dependence of the Cr³⁺ EPR signal when the magnetic field is rotated in the (*ab*) plane and the (*bc**) plane, respectively. The experimental data are shown by the open circles, while the simulation results using the spin-Hamiltonian in Eq.1 are depicted by the solid lines. All measurements were done at 6K. The signals marked by (*) originate from an empty microwave cavity, unrelated to the sample.

Figure 2: (a) Representative PL spectra from the investigated β -Ga₂O₃ crystals measured at 7K and 300K. Magneto-PL spectra measured at 5K under an applied magnetic field (varying from 0 to 5 T) parallel to the crystallographic *a*-axis (b), *b*-axis (d) and *c**-axis (c). (e) Energy difference Δ E between the two spin sublevels of the first excited state, i.e. the Zeeman splitting, as a function of **B**. The inset in (e) shows the PL spectra measured at 5K and 20K at 5T with **B** || *a*. The transitions are labeled as 1 - 8, in the order of increasing energy.

Figure 3: Energy level splitting of the Cr^{3+} ground state with an applied magnetic field along the crystallographic *a*-axis (a), *b*-axis (b) and c^* -axis (c). The open circles are the experimental data from the magneto-PL experiments. The solid lines are simulation results using Eq. 1 and the parameters obtained from the EPR measurements (given in Table 1).

Figure 4: Electronic structure and spin configuration of Cr^{3+} in β -Ga₂O₃ with and without an

applied magnetic field \mathbf{B} . The solid red and orange arrows labeled as R1 and R2, respectively, indicate the optical transitions from the two Kramers' doublets of the ${}^{2}\mathrm{E}$ state to the ${}^{4}\mathrm{A}_{2}$ ground state at \mathbf{B} =0. The ${}^{4}\mathrm{A}_{2}$ ground state also experiences ZFS, indicated by δ , which gives rise to the fine structure of the R-lines. Under an applied magnetic field (\mathbf{B} \neq 0), both the ground and excited states further split due to the removal of their spin degeneracy. Therefore, a maximum of eight optical transitions can be observed for the R1 emission. They are labeled as 1-8 corresponding to that used in the magneto-PL data. The spin sublevels of the ground state are indicated by a magnetic quantum number m_{s} , representing the corresponding spin state under a high-field condition for simplicity.